EUROPEAN FUSION DEVELOPMENT AGREEMENT

EFDA–JET–PR(04)55

Yueqiang Liu, A. Bondeson, M.S. Chu, J-Y. Favez, Y. Gribov,
M. Gryaznevich, T.C. Hender, D.F. Howell, R.J. La Haye, J.B. Lister
and JET EFDA contributors

Feedback and Rotational Stabilization of Resistive Wall Modes in ITER

Feedback and Rotational Stabilization of Resistive Wall Modes in ITER

Yueqiang Liu[1], A. Bondeson[1], M.S. Chu[2], J-Y. Favez[3], Y. Gribov[4], M. Gryaznevich[5], T.C. Hender[5], D.F. Howell[5], R.J. La Haye[2], J.B. Lister[3] and JET EFDA contributors*

[1]Department of Electromagnetics, EURATOM/VR Fusion Association, Chalmers University of Technology, G¨oteborg, Sweden
[2]General Atomics, San Diego, CA, USA
[3]CRPP, Ecole Polytechnique F´ed´erale de Lausanne, Switzerland
[4]Physics Unit, ITER Naka Joint Work Site, Naka, Ibaraki, Japan
[5]Euratom/UKAEA Fusion Association, Culham Science Centre, Abingdon, UK
** See annex of J. Pamela et al, "Overview of Recent JET Results and Future Perspectives", Fusion Energy 2002 (Proc.19 th IAEA Fusion Energy Conference, Lyon (2002).*

Preprint of Paper to be submitted for publication in
Nuclear Fusion

ABSTRACT.
Different models have been introduced in the stability code MARS-F in order to study the damping effect on Resistive Wall Modes (RWM) in rotating plasmas. Benchmark of MARS-F calculations with RWM experiments on JET and DIII-D indicates that the semikinetic damping model is a good candidate for explaining the damping mechanisms. Based on these results, the critical rotation speeds required for RWM stabilization in an advanced ITER scenario are predicted. Active feedback control of the n = 1RWM in ITER is also studied using the MARS-F code.

1. INTRODUCTION

One of the major limiting factors for achieving high beta in advanced tokamaks is the onset of Resistive Wall Modes (RWM). These are usually pressure driven, low n, external kink modes, whose growth rates are greatly suppressed by surrounding conducting walls. The modes become unstable as soon as the plasma pressure exceeds the no-wall ideal limit, with a growth time of order the wall eddy current decay time. Therefore, the RWM must be stabilized in order to achieve steady state operations and high plasma pressures in ITER advanced scenarios.

Two possible approaches have been proposed to stabilize the RWM: toroidal plasma rotation and active feedback. It has been shown, in both theory [1,2] and experiments in DIII-D [3,4,5], that the RWM can be completely stabilized by plasma rotation, provided that the rotation speed exceeds certain critical value, which is typically a few percent of the Alfvén frequency. Since it is probably not possible to maintain a very fast rotation in ITER plasmas, the rotation speed for RWM stabilization in ITER is a critical issue. Calculations using MARS-F code [6] show that the critical rotation depends sensitively on the damping models. This paper reports detailed benchmarking of the damping models against the experimental results in JET and DIII-D. These benchmark results allow us to choose a good damping model for the ITER prediction.

The possibility of stabilizing the RWM using feedback control has been actively exploited during the recent years, both in theories [7,8,9,10,11,12,13,14] and experiments [15,16,17]. In previous papers, e.g, [6,18], we have shown that active stabilization for tokamaks works best when sensors for the poloidal field are placed inside the first wall. Robust stabilization of pressure-driven n = 1 kinks can be achieved, by using a single array of coils, located poloidally at the outboard midplane, where the modes balloon [18]. Recently MARSF has been used to study active control of RWM for the present ITER design [19]. This paper studies the possibility of improving the feedback control for ITER plasmas, by choosing better sensor signals, and by using internal feedback coils, as opposed to the external coils in the present ITER design.

2. ROTATIONAL STABILIZATION

2.1. DAMPING MODELS

A key issue in understanding the physics of RWM in a rotating plasma is the damping mechanism. It was suggested some time ago [1], and verified with recent experiments [5], that besides the

Alfvén continuum damping, the ion Landau damping also plays an important role in suppressing the mode.

In the MARS-F code, the ion Landau damping is modeled in two ways. One is the parallel sound wave damping, where a viscosity force,

$$\vec{F}_{visc} = -\kappa_{||} | k_{||} | \; v_{,i} \rho \vec{v}_{||} \;, \tag{1}$$

for each (m,n)-component of the helical perturbations, is added to the momentum equation (in the single fluid MHD setup) along the parallel motion. In Eq. (1), $\kappa_{||}$ $(m/q - n)/R$ is the parallel wave number, $v_{th,\,i}$ is the ion thermal velocity, ρ is the mass density, and $\vec{v}_{||}$ is the perturbed parallel velocity of the plasma. The drawback of this model is the presence of an adjustable parameter $\kappa_{||}$.

The other model follows a simplified drift-kinetic large-aspect-ratio analysis [20], where the kinetic energy perturbations are computed taking into account the contributions from both circulating and trapped particles.

$$\Delta W_T = \frac{1}{2} \sum_{m'} \int d^3 x \int_{trapped} d\Gamma \left(-\frac{\partial f}{\partial E} \right) \frac{\omega}{\omega + m'\omega_b} \left| <\exp(j\,\chi m')H> \right|^2 , \tag{2}$$

$$\Delta W_T = \frac{1}{2} \sum_{m'} \int d^3 x \int_{circ} d\Gamma \left(-\frac{\partial f}{\partial E} \right) \frac{\omega}{\omega - (nq - m')\omega_t} \left| <\exp(j\,\chi m')H> \right|^2 . \tag{3}$$

In Eq. (2)-(3), f is the Maxwellian distribution, E is the particle energy, n the toroidal mode number, m' the bounce harmonics, ω_b the bounce frequency of the trapped particles, and ω_t the transit frequency of the passing particles. ω is the real frequency of the mode with respect to the plasma. For RWM studies, we adopt the plasma rotation frequency for ω. The quantities $\chi' m$ are defined as phase factors for passing and trapped particles, respectively. The quantity H is the perturbation of a particle's energy, which is determined by the perturbation of the magnetic field strength together with the field line curvature.

The imaginary part (responsible for damping) of the kinetic $\Delta W = \Delta W_T + \Delta W_C$ is evaluated and the equivalent damping force F_{diss} is computed via the relation

$$jIM(\Delta W_C + \Delta W_T) = -\frac{1}{2} \int \vec{F}_{diss} \cdot \vec{\xi}^*_{\perp} d^3 x . \tag{4}$$

As shown in Eq. (4), the added damping force acts on the perpendicular motion. Due to the toroidal coupling, the m component of the field perturbation $\vec{b}$ couples to the $m \pm 1$ components of the parallel motion. This coupling makes the Landau damping rather nonlocal. For example, even at $\omega \sim 0.02\omega_A$, the momentum transfer is spread out over entire plasma, as shown in Fig. 1. Here we plot the damping coefficients D_C and D_T, defined in Ref. [20] and computed by MARS-F for the equilibrium and the rotation pro le from a DIII-D Pulse. Figure 1(d) shows the kinetic damping energy density (the integrant in Eq. (4)) along the radial direction for different poloidal Fourier

harmonics. Such a rather global distribution of the damping energy explains the 'strong' damping effect from the kinetic model, as will be shown in the following sections.

The present kinetic damping model neglects the effects of finite diamagnetic and gyrocenter drift frequencies ($\omega_* = \omega_d = 0$). Also, the electrostatic potential is assumed to be zero. Some of these effects may be of importance for more appropriate modeling [21], and will be included into the MARS-F code in the future.

2.2. CRITICAL ROTATION VELOCITY

Using two damping models, we computed the critical rotation speeds for two series of equilibria based on JET Pulse No: 62366 and DIII-D Pulse No: 109174. The chosen JET equilibria have q_{95} around 4.8, and the DIII-D equilibria have q_{95} around 3.6. Shown in Fig.2(a-b) is the comparison of the MARS-F calculations with the experimental data. The critical rotation is plotted against the plasma pressure, which is described by a parameter $C_\beta \equiv (\beta_N - \beta_N^{\text{no-wall}})/(\beta_N^{\text{ideal-wall}} - \beta_N^{\text{no-wall}})$.

The kinetic damping, as well as the sound wave damping with $\kappa_{||} = 1-1.5$, gives good prediction for JET plasmas, when compared with initial experimental results [22]. For DIIID, the kinetic damping model underestimates the critical rotation by about 40%, whereas the sound wave damping model with $\kappa_{||} = 0.1$ overestimates the critical rotation by about 40%. It should be noted that for both JET and DIII-D, the dependence of critical rotation on the plasma pressure is not sensitive. Such behavior is correctly recovered by the kinetic damping model.

Figure 2 also shows that the critical rotation in JET is generally 2-4 times smaller than that in DIII-D. Such a difference is observed in both experimental data and in MARS-F calculations. In order to resolve the possible cause for this, we made calculations for a series of equilibria varying from JET to DIII-D. Shown in Fig.3 is the computed critical rotation for four equilibria, using the kinetic damping model. Eq.1 is a JET equilibrium reconstructed from Pulse No: 62653 at 6.68s, with the JET plasma rotation profile, Eq.4 a DIII-D equilibrium from Pulse No: 109174, with the DIII-D rotation profile. Eq.2 is the same JET equilibrium but with DIII-D rotation pro le. Eq.3 has the current density (and pressure) profile from JET, but the plasma and wall shapes as well as the rotation pro le from DIII-D. For the specific cases studied here, the plasma rotation profile has much less in uence on the critical rotation, than the plasma and wall shapes. The wall in JET is relatively farther away and the spread in beta between the no wall and ideal wall limits is smaller in JET than in DIII-D. The current density profiles (the q-profiles) also have significant in uence on the critical rotation. In this study, both the JET and DIII-D equilibria have similar q_{95} – about 3.4 for JET and about 3.6 for DIII-D. For the 'intermediate' equilibria, we keep the q_{95} to be 3.4 by scaling the total plasma current. For all four cases, the C_β values are approximately 0.5. It should be pointed out that the measured critical rotation for this JET shot is about twice larger than the value computed by MARS-F. Such a discrepancy, as well as the discrepancy observed for DIII-D modeling, indicates that further improvement of the damping models is necessary.

For fixed equilibrium profiles and shapes, we found that the critical rotation has strong dependence on q_{95}. Figure 4 collects all the *computed* data for various equilibria from JET, DIII-D and ITER.

All the equilibria have C_β at about 50-60%. For a given experimental shot (i.e., with fixed equilibrium current and pressure profiles, the rotation profile, the plasma and wall shapes), q_{95} is scaled by varying the total plasma current.

As shown in Fig.4, the critical rotation velocity generally increases with decreasing q_{95}. This indicates that, at high-q discharges, the damping from the plasma edge may also be important for the RWM stabilization. For a fixed shot, the scaling is rather linear with respect to $1/q^2_{95}$, which agrees with the theory [20]. Of course, the critical rotation varies between different machines, as shown by Fig.3. Nevertheless, the scaling shown in Fig.4 is in favor of high-q equilibria with high bootstrap fraction.

2.3. RESONANT FIELD AMPLIFICATION

Resonant Field Amplification (RFA) has been extensively exploited in DIII-D [23,24] and JET [22] experiments. These experiments can be viewed as MHD spectroscopy for rotationally stabilized RWM. Hence they also offer an excellent benchmark for the damping models.

We have pursued a systematic analysis of RFA experiments in JET using MARSF [25,22]. This analysis shows that (1) the computed amplitude and phase of the field amplification depend sensitively on the damping models used in MARS-F; (2) kinetic damping gives reasonable agreement with the experimental data, for both internal and external saddle coils, with excitation currents in the form of both DC pulses and standing waves.

As an example, Fig.5 shows the computed total response of the plasma and the wall to the applied error field from internal saddle coils. We plot, in the complex plane, the amplified field excited by traveling waves with various frequencies. The response is normalized by the vacuum field produced by a DC current. For comparison, the vacuum response (i.e. without plasma) of the conducting wall is also plotted. The computed results (denoted by circles) are approximated by second order rational functions (solid lines)

$$P_{RFA}(j\omega_c) = \frac{1.008 + j0.535}{j\omega_c + 0.884 - j0.281} + \frac{0.045 + j0.031}{j\omega_c + 0.176}, \tag{5}$$

$$P_{VACUUN}(j\omega_c) = \frac{0.911}{j\omega_c + 1} + \frac{0.021}{j\omega_c + 0.164}, \tag{6}$$

where ω_c is the traveling wave frequency normalized by the wall time. Figure 5 and Eqs.(5)-(6) show that, with internal saddle coils, the plasma indeed modifies and amplifies significantly the error fields, measured by pick-up coils located along the outboard midplane outside the vacuum vessel.

2.4. ITER PREDICTION

The benchmark study with JET and DIII-D experiments on critical plasma rotation and RFA indicates that the kinetic damping can be a good candidate for describing the damping physics for RWM. This allows us, with certain con dence, to predict the critical rotation for the RWM stabilization in ITER plasmas.

We consider a steady state scenario for ITER (Scenario-4 from the ITER design) [19]. Figure 6 shows the computed growth rates of the n = 1 RWM, with increasing the rotation amplitude and fixing the rotation profile, which is predicted by transport calculations using the ASTRA code [26]. The critical rotation frequency, predicted by the kinetic damping model, varies between 1.5-3%ω_A at the plasma center. Since the predicted (by ASTRA) ITER plasma rotation is less than 2%ω_A at the plasma center, we conclude that rotational stabilization alone may not be robust for the RWM in ITER. Active control of the mode using feedback may be required.

3. FEEDBACK STABILIZATION

3.1. CHOICE OF FEEDBACK LOGIC

For feedback control of ITER plasmas, we choose so-called voltage-to-voltage control

$$V_f = KV_s,$$

where K is the controller. The voltages of the feedback coil (V_f) and the sensor loop (V_s) are defined as

$$V_f = \frac{d\psi_f}{dt}, \quad V_s = \frac{L_f}{M_{sf}} \frac{d\psi_s}{dt},$$

where ψ_f is the flux through the feedback coil, ψ_s the flux through the sensor loop, L_f the self-inductance of the feedback coil, and M_{sf} the mutual inductance between the feedback and sensor coils. The resistance of the feedback coil is neglected since ITER has superconducting coils.

We introduce two transfer functions that completely describe the plasma response from the MHD calculations

$$P_1 = \frac{\psi_s}{M_{sf} I_f}, \quad P_2 = \frac{\psi_f}{L_f I_f}.$$

The total plasma response is thus determined by the transfer function $P=P_1/P_2$. The feedback coil in the present ITER design is rather far from the plasma (at radial distance of about 3a, where a the plasma minor radius). As a consequence, P_2 is typically close to 1.

3.2. CHOICE OF SENSORS

As has been pointed out earlier [8, 6], feedback stabilization of the RWM is sensitive to the choice of sensor signals. A good choice is the poloidal field component inside the vacuum wall at the outboard midplane [6]. This is denoted as internal poloidal sensors. Other possible choices are external poloidal sensors (i.e. poloidal sensor outside the wall), radial sensors (typically on the wall), radial sensors with compensation of the vacuum coil fields, and various combinations of these sensors [11]. Quite often, the best choice turns out to be internal poloidal sensors alone. We illustrate this by studying a feedback system for a cylindrical plasma with the current density profile as a step function. In this case the transfer function P, including all poloidal harmonics, can be computed analytically [27] for all types of sensor signals. Let us denote the corresponding transfer functions as P_r, P_p, P_{p+}, P_c for radial, internal poloidal, external poloidal sensors and for vacuum coils without the plasma but with the wall, respectively.

We define $P_{tot} \equiv C_r P_r + C_{p-} P_{p-} + C_{p+} P_{p+} + C_c P_c$ as the transfer function for combined sensors, and minimize the control activity (approximately a measure of the feedback gain) $\|KS\|_\infty \equiv \sup_\omega |K(j\omega)/(1+K(j\omega)P_{tot}(j\omega))|$ with respect to a PD controller $K(s) = K_p(1+ T_d s)=(1+T_d s/\xi)$, where ω is the real frequency, s the Laplace transform variable, and K_p, T_d, ξ controller parameters to be optimized. Figure 7 shows the minimized $\|KS\|_\infty$ versus parameter C_r, for three interesting combinations of the sensor signals. The best result is achieved by choosing $C_{p-} = 1$, $C_r = C_{p+} = C_c = 0$, i.e. by using only internal poloidal sensors. Thus for feedback study of the RWM in ITER, we consider mainly internal poloidal sensors. In addition, a compensation scheme for these sensors is also proposed in Section 3.4.

3.3. CHOICE OF FEEDBACK COILS

The present ITER design uses the side correction coils for the RWM feedback control. These are superconducting coils, located along the outboard midplane and external to the ITER walls, with three pairs of toroidally opposite coils connected to produce the $n = 1$ magnetic field.

Using MARS-F, we compute the transfer functions P_1 for the designed equilibria in ITER Scenario-4, using internal poloidal sensors for feedback. These functions are then approximated (in frequency domain) with 2- or 3-pole rational functions. Shown in Fig. 8(a) are the transfer functions $P_1(j\omega)$ in the complex plane for real frequencies ω and for various plasma pressures. The closed-loop system will be stable, if the open-loop curve for $K(j\omega)P_1(j\omega)$ ($K = 1$ in Fig. 8) encircles -1 once counterclock-wise. For example, with a proportional gain $K = K_p = 1.3$, the curve $K_p P_1$ for $C_\beta = 60\%$ will eventually encircle -1 once counter-clock-wise, thus the closed loop for $C_\beta = 60\%$ will be stable with $K_p = 1.3$. One can see that with large enough proportional gains $K = K_p$, the RWM can be stabilized for C_β value at least up to 60%. By adding appropriate derivative action, the mode can be stabilized even at higher plasma pressures. Here we assume that the feedback system has ideal amplifiers (i.e. amplifiers with infinite bandwidth).

Figure 8(b) shows the computed transfer functions $P_1(j\omega)$ if we move the feedback coils just inside the ITER inner wall. As expected, the control becomes much easier with internal feedback coils. A large enough proportional gain in this case stabilizes the RWM for C_β close to 1 (the ideal wall limit). Also, the performance of the control is better because of the larger phase of $P_1(j\omega)$.

3.4. CONTROL OPTIMIZATION FOR ITER

As shown in Fig. 8(a), the present design of feedback coils allow stabilization of the $n = 1$ RWM up to $C_\beta = 60\%$ using internal poloidal sensors and only proportional gains. Better results can be achieved by using optimally tuned PID controllers and improved sensor signals. We choose a PID controller

$$K(s) = (K_p + \frac{K_i}{s}) \frac{1+T_d s}{1+T_d s/\xi'}$$

and optimize four parameters $\{K_p, K_i, T_d, \xi\}$ to achieve minimum peak voltage for a reference event where the controller is turned on after the field reaches 1.5mT, subject to constraints on stability parameter

$$J_s \equiv \| \frac{1}{1+K(j\omega)P1(j\omega)} \|_\infty$$

and the settling time τ_{set}. The value $1/J_S$ measures the distance of the (stabilized) closed loop to the marginal stability. The value τ_{set} measures how quickly the feedback system stabilizes the mode. In Fig.9, the maximal voltages are plotted against C_β, for three sets of constraints, corresponding to three curves with 'o'. With the design voltage limit of 300 V/turn for the amplifier, the RWM can be controlled with good performance ($J_S = 2$, $\tau_{set} / \tau_\omega = 1$) for $C_\beta \lesssim 65\%$, and with moderate performance ($J_S = 2.5$, $\tau_{set} / \tau_\omega = 2$) for $C_\beta < 70\%$. The peak voltage can be further decreased if we use internal poloidal sensor signals compensated by a signal $P_c(s) = T_{d2} / (s+\xi_2)$, where parameters T_{d2} and ξ_2 are optimally chosen and are the same for all pressures. The results are presented by three curves with '+' in Fig. 9. Using this technique, the RWM can be stabilized, with good performance, up to $C_\beta \gtrsim 80\%$. We mention that similar results have been achieved in [28] using the plasma response models computed by MARS-F.

4. CONCLUSION

Two damping models have been benchmarked against the present experimental data for RWM study. The semi-kinetic damping model gives reasonable results for both critical plasma rotation required for the RWMstabilization, and the RFA experiments. Such a model predicts that the critical rotation frequency for stabilizing the $n = 1$ RWM in ITER is about 1.5-3%ω_A at the plasma center. Further improvement of the kinetic damping model, by including more physics, is needed for better prediction.

With the present coil design in ITER for feedback control, it is possible to stabilize the $n = 1$ RWM for plasma pressures up to 80% between the no-wall and ideal-wall limits, using optimally tuned PID controllers and optimally compensated internal poloidal sensor signals. The control can be further improved by using internal feedback coils. Finally, more robust stabilization of the RWM in ITER is possible by combining feedback and plasma rotation [19].

For more realistic prediction of the feedback performance in ITER, other issues such as 3D wall effect, system noise, the superconducting coil AC losses, need to be addressed. These issues will be studied in the future.

ACKNOWLEDGEMENTS

This work was conducted under the European Fusion Development Agreement and partly funded by EURATOM, VR and the US DOE.

REFERENCES

[1]. A. Bondeson, and D.J. Ward, Phys. Rev. Lett. 72 2709 (1994).

[2]. D. Gregoratto, et al., Plasma Physics and Controlled Fusion **43** 1425 (2001).

[3]. A.M. Garofalo, et al, Phys. Rev. Lett. **82** 3811 (1999).

[4]. A.M. Garofalo, et al., Phys. Plasmas **9** 1997 (2002).

[5]. R.J. La Haye, et al, Nucl. Fusion **44**, 1197 (2004).

[6]. Y.Q. Liu, et al., Phys. Plasmas **7**, 3681 (2000).

[7]. R. Fitzpatrick, Yu, E.P., Phys. Plasmas **6**, 3536 (1999).

[8]. Y.Q. Liu and A. Bondeson, Phys. Rev. Lett. **84** 907 (2000).

[9]. J. Bialek, et al., Phys. Plasmas **8**, 2170 (2001).

[10]. A. Bondeson, et al., Phys. Plasmas **9**, 2044 (2002).

[11]. V.D. Pustovitov, Plasma Phys. Control. Fusion **44**, 295 (2002).

[12]. M.S. Chu, et al, Nucl. Fusion **43** 441 (2003).

[13]. A.H. Boozer, Phys. Plasmas **11** 110 (2004).

[14]. J.M. Finn, Phys. Plasmas **11** 4361 (2004).

[15]. A.M. Garofalo, et al, Nucl. Fusion **41** 1171 (2001).

[16]. M. Okabayashi, et al., Phys. Plasmas **8** 2071 (2001).

[17]. E.J. Strait, et al, Nucl. Fusion **43** 430 (2003).

[18]. Y.Q. Liu, et al, Nucl. Fusion **44** 77 (2004).

[19]. Y.Q. Liu, et al, Nucl. Fusion **44** 232 (2004).

[20]. A. Bondeson and Chu M.S., Phys. Plasmas **3** 3013 (1996).

[21]. B. Hu and R. Betti, Phys. Rev. Lett. **93**, 105002 (2004).

[22]. T.C. Hender, et al, "Resistive Wall Mode Studies in JET", EX/P2-22, 20th IAEA Fusion Energy Conference, Vilamoura, Portugal, 1-6 November 2004.

[23]. A.M. Garofalo, et al, Phys Plasmas **10**, 4776 (2003).

[24]. H. Reimerdes, et al, Phys. Rev. Lett. **93**, 135002 (2004).

[25]. Y.Q. Liu, et al, "Modeling of Resistive Wall Mode Experiments in JET", Preceeding of 30th EPS Conference on Plasma Phys. and Contr. Fusion, Imperial College, UK, 2004.

[26]. A. Polevoi et al., Fusion Energy 2002 (Proc. 19th Int. Conf. Lyon, 2002) (Vienna: IAEA) CD-ROM le CT/P-08 and http://www.iaea.org/programmes/ripc/physics/fec2002/html/fec2002.htm

[27]. A. Bondeson, et al., Nucl. Fusion **42** 768 (2002).

[28]. Y. Gribov and A. Kavin, "Study of ITER RWM control with semi-analytical models", IT/P3-22, 20th IAEA Fusion Energy Conference, Vilamoura, Portugal, 1-6 November 2004.

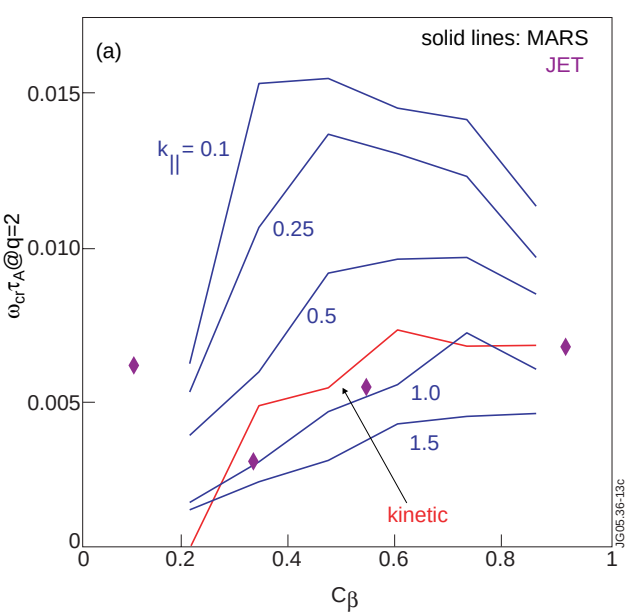

Figure 1: The kinetic damping energy computed by MARS-F for the equilibrium and the experimental rotation from a DIII-D discharge 109174. The damping coef cients D_C and D_T, defined in Ref. [20], are proportional to the imaginary part of the kinetic energy perturbation. Ψ_n denotes the normalized poloidal flux. (a) - contribution from circulating particles, (b) - contribution from trapped particles, (c) total contributions, (d) the volume density of the computed kinetic damping energy.

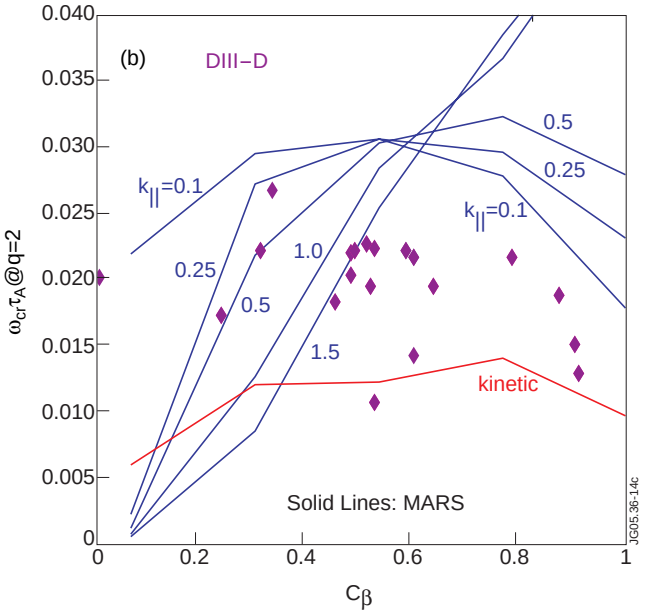

Figure 2: The critical rotation frequency at the q=2 surface, normalized by Alfvén frequency, versus the plasma pressure characterized by C_β ($\beta_N - \beta_N^{no-wall}$)/ ($\beta_N^{ideal-wall} - \beta_{Nn}^{no-wall}$). Plotted are experimental data (dots) and the MARS-F results (solid curves) with parallel sound wave damping and semi-kinetic damping models, (a) - for JET, (b) - for DIII-D.

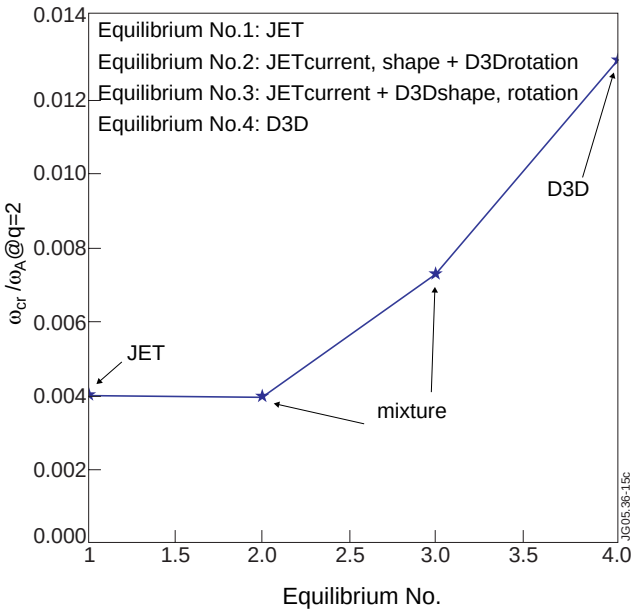

Figure 3: The critical rotation velocity computed for a series of equilibria varying from JET to DIII-D. The C_β and q_{95} are kept approximately the same for all equilibria.

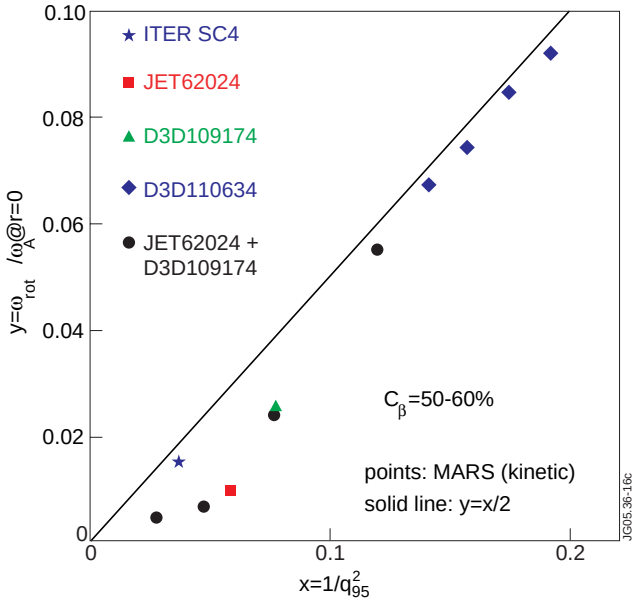

Figure 4: The critical rotation velocity computed for various equilibria using MARS-F with the kinetic damping model (dots). Plotted is the critical rotation frequency at the plasma center versus q_{95}.

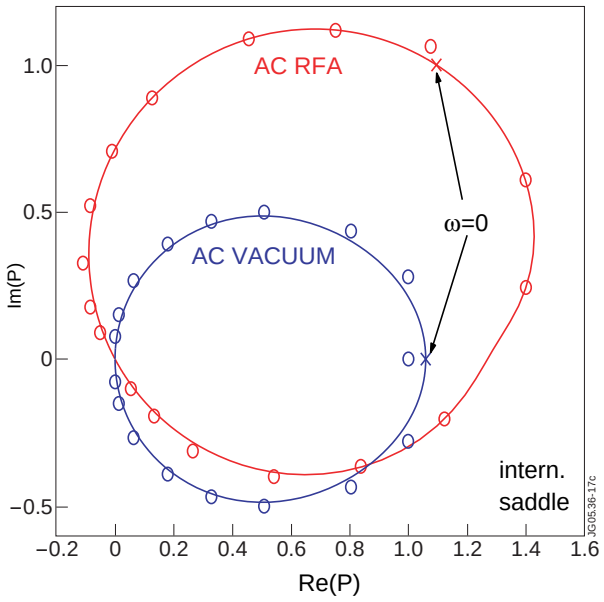

Figure 5: The complex plot of the computed plasma response to traveling waves launched by internal saddle coils in JET. The vacuum response is also plotted for comparison.

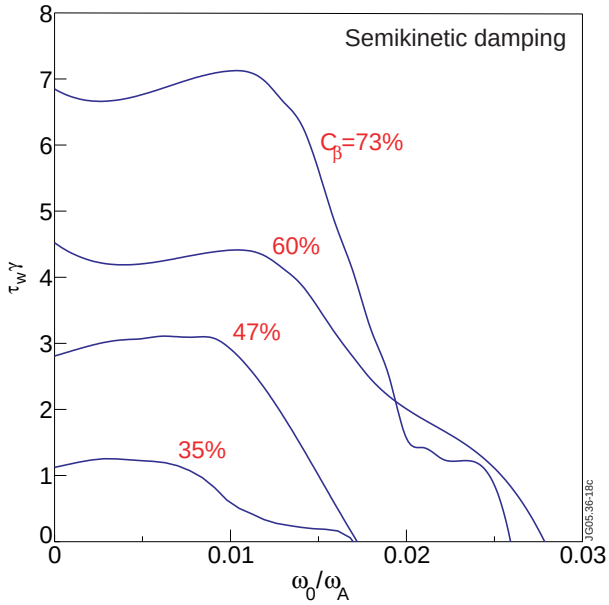

Figure 6: The computed growth rates of the RWM in ITER advanced scenario-4 for various plasma pressures. The central plasma rotation frequency ω_0 is normalized by the Alfvén frequency ω_A. The semi-kinetic damping model is used.

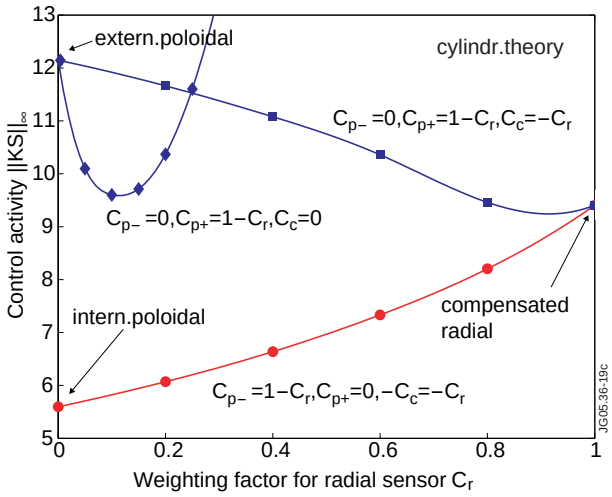

Figure 7: Controller optimization for various combinations of sensor signals. Results are obtained for a cylindrical plasma.

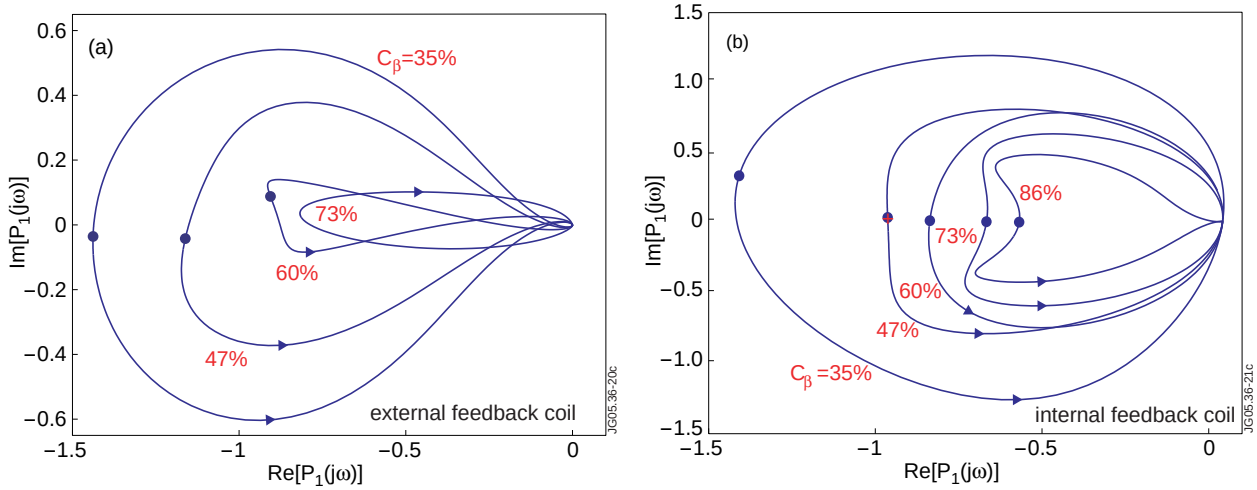

Figure 8: The transfer functions $P_1(j\omega)$, for real frequencies ω, plotted in the complex plane for various plasma pressures for (a) external feedback coils in the ITER design, and (b) assumed internal feedback coils.

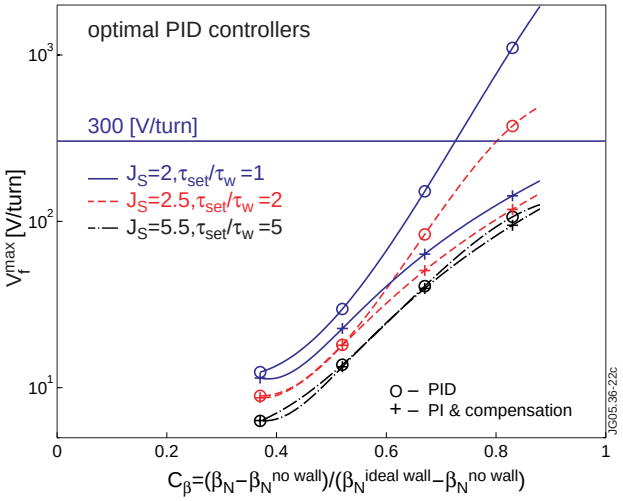

Figure 9: The maximum voltage required to stabilize the RWM versus the plasma pressure, with various sets of control performace speci cations and with two different control schemes. The value $1/J_S$ measures the distance of the (stabilized) closed loop to the marginal stability. The value τ_{set} measures how quickly the feedback system stabilizes the mode. The ITER design voltage limit for the power amplifier is 300V/turn.